OPEN

High Structural Stress and Presence of Intraluminal Thrombus Predict Abdominal Aortic Aneurysm ^{18}F-FDG Uptake

Insights From Biomechanics

Yuan Huang, PhD; Zhongzhao Teng, PhD; Maysoon Elkhawad, MD; Jason M. Tarkin, MBBS; Nikhil Joshi, MD; Jonathan R. Boyle, MD, FRCS; John R. Buscombe, MB ChB, MD; Timothy D. Fryer, PhD; Yongxue Zhang, MD, PhD; Ah Yeon Park, PhD; Ian B. Wilkinson, MA, DM, FRCP; David E. Newby, MD; Jonathan H. Gillard, MD; James H. F. Rudd, MD, FRCP, PhD

Background—Abdominal aortic aneurysm (AAA) wall inflammation and mechanical structural stress may influence AAA expansion and lead to rupture. We hypothesized a positive correlation between structural stress and fluorine-18-labeled 2-deoxy-2-fluoro-D-glucose (^{18}F-FDG) positron emission tomography–defined inflammation. We also explored the influence of computed tomography–derived aneurysm morphology and composition, including intraluminal thrombus, on both variables.

Methods and Results—Twenty-one patients (19 males) with AAAs below surgical threshold (AAA size was 4.10±0.54 cm) underwent ^{18}F-FDG positron emission tomography and contrast-enhanced computed tomography imaging. Structural stresses were calculated using finite element analysis. The relationship between maximum aneurysm ^{18}F-FDG standardized uptake value within aortic wall and wall structural stress, patient clinical characteristics, aneurysm morphology, and compositions was explored using a hierarchical linear mixed-effects model. On univariate analysis, local aneurysm diameter, thrombus burden, extent of calcification, and structural stress were all associated with ^{18}F-FDG uptake (P<0.05). AAA structural stress correlated with ^{18}F-FDG maximum standardized uptake value (slope estimate, 0.552; P<0.0001). Multivariate linear mixed-effects analysis revealed an important interaction between structural stress and intraluminal thrombus in relation to maximum standardized uptake value (fixed effect coefficient, 1.68 [SE, 0.10]; P<0.0001). Compared with other factors, structural stress was the best predictor of inflammation (receiver-operating characteristic curve area under the curve =0.59), with higher accuracy seen in regions with high thrombus burden (area under the curve =0.80). Regions with both high thrombus burden and high structural stress had higher ^{18}F-FDG maximum standardized uptake value compared with regions with high thrombus burdens but low stress (median [interquartile range], 1.93 [1.60–2.14] versus 1.14 [0.90–1.53]; P<0.0001).

Conclusions—Increased aortic wall inflammation, demonstrated by ^{18}F-FDG positron emission tomography, was observed in AAA regions with thick intraluminal thrombus subjected to high mechanical stress, suggesting a potential mechanistic link underlying aneurysm inflammation. **(*Circ Cardiovasc Imaging*. 2016;9:e004656. DOI: 10.1161/CIRCIMAGING.116.004656.)**

Key Words: abdominal aortic aneurysm ■ fluorodeoxyglucose F18 ■ inflammation ■ mechanical stress ■ positron-emission tomography ■ thrombosis

Abdominal aortic aneurysm (AAA) is a localized enlargement of the aorta, conventionally diagnosed when the maximum anteroposterior vessel diameter exceeds 3.0 cm.[1] AAAs are most prevalent in elderly men and are frequently asymptomatic until point of rupture, which is the catastrophic failure of the aneurysmal wall associated with an overall mortality rate between 65% and 85%.[2] Current management is

See Editorial by Curci and Beckman
See Clinical Perspective

Received February 2, 2016; accepted September 19, 2016.

From the Department of Radiology (Y.H., Z.T., Y.Z., J.H.G.), EPSRC Centre for Mathematical and Statistical Analysis of Multimodal Clinical Imaging (Y.H.), Department of Engineering (Z.T.), Division of Cardiovascular Medicine (M.E., J.M.T., I.B.W., J.H.F.R.), Wolfson Brain Imaging Centre (T.D.F.), and Statistical Laboratory (A.Y.P.), University of Cambridge, United Kingdom; British Heart Foundation Centre for Cardiovascular Science, University of Edinburgh, United Kingdom (N.J., D.E.N.); Department of Vascular Surgery (J.R. Boyle) and Department of Nuclear Medicine (J.R. Buscombe), Addenbrooke's Hospital, Cambridge, United Kingdom; and Department of Vascular Surgery, Changhai Hospital, Shanghai, China (Y.Z.).

The Data Supplement is available at http://circimaging.ahajournals.org/lookup/suppl/doi:10.1161/CIRCIMAGING.116.004656/-/DC1.

Correspondence to Zhongzhao Teng, PhD, Department of Radiology, University of Cambridge, Box 218 Cambridge Biomedical Campus, Hills Rd, Cambridge CB2 0QQ, United Kingdom. E-mail zt215@cam.ac.uk or James H. F. Rudd, MD, FRCP, PhD, Department of Medicine, University of Cambridge, Box 110, Addenbrooke's Centre for Cardiovascular Investigation, Hills Road, Cambridge CB2 2QQ, United Kingdom. E-mail jhfr2@cam.ac.uk

largely based on serial imaging to determine the maximum baseline diameter and rate of growth, with open or endovascular repair typically recommended for AAAs >5.5 cm. However, clinical trials and autopsy studies suggest that some small- and medium-sized AAAs will also rupture, whereas some large aneurysms can remain static for many years.[3] Thus, aneurysm diameter alone cannot reliably identify high-risk AAAs, highlighting the need of better risk stratification.

AAAs result from pathological changes occurring within the aortic wall that lead to tissue degradation and smooth muscle cell apoptosis; often adventitial and transmural inflammatory cell infiltrates are seen when examined histologically.[4,5] These pathological changes are associated with AAA expansion and rupture,[6,7] and inflammation in particular may cause extensive media damage.[8,9] To quantify aortic wall inflammation in patients with aneurysm, fluorine-18-labeled 2-deoxy-2-fluoro-D-glucose (^{18}F-FDG) positron emission tomography (PET) has been described.[10,11] It enables detection of the increased glucose metabolic rate that is characteristic of aortic wall inflammation.[5]

Pulsatile loading because of changes in blood pressure and flow under physiological conditions also contribute to the pathogenesis of AAA, in part because of extracellular matrix breakdown.[12,13] Ultimately, AAA rupture occurs when forces within the AAA structure exceed its inherent tissue strength. Biomechanical analysis can be applied to evaluate risks of AAA rupture[14,15] by modeling structural stress, derived from several factors including aneurysm morphology and composition with excellent intra-/interobserver reproducibility.[16] The overall relationship between structural stress and AAA inflammation has been studied by several groups.[17–19] However, other aneurysm components, including intraluminal thrombus (ILT) and calcium, have only been partially considered in previous studies. In addition, the possible coinfluence of structural stress and aneurysm architectural features on ^{18}F-FDG uptake remains unexplored. In this study, we aimed to quantify the distribution of structural stress within AAAs, modeling the effect of both calcification and ILT, and the association between local ^{18}F-FDG uptake and structural stress, AAA morphology, and composition.

Methods

PET-CT Imaging

Patients with AAA were recruited from Cambridge University Hospitals, United Kingdom. The inclusion criteria were age >50 years and presence of an aneurysm between 3.0 and 5.5 cm. Exclusion criteria were insulin-dependent diabetes mellitus, type 2 diabetes mellitus with a fasting glucose of >11 mmol/L, any disease expected to shorten life expectancy to <2 years, women of childbearing age not taking contraception, severe renal failure (serum creatinine >250 μmol/L), known contrast allergy, or the inability to provide informed consent. All subjects provided written informed consent in accordance with the research protocol approved by the local institutional review board (MREC 09/H0308/27). All patients underwent ^{18}F-FDG PET-computed tomography (CT) imaging of the aorta using a GE Discovery 690 PET/CT scanner (GE Healthcare). The details of imaging protocol are provided in Material in the Data Supplement.

AAA Segmentation and Finite Element Simulation

AAA segmentation was performed using contrast-enhanced aortic CT images (Figure 1A and 1D). The luminal contour was delineated using a region-growing algorithm, and the outer wall was segmented manually. Because of the poor contrast between ILT and wall in CT image, the outer boundary of ILT was obtained by uniformly shrinking the wall contour inward with the assumption of constant wall thickness[17] and the region enclosed by this shrunk wall contour and lumen boundary was defined as ILT (Figure 1D). Calcium was segmented using relative signal intensity,[20] with different percentage threshold from 100% to 160% in steps of 5% with reference to the mean lumen signal intensity. The results were then compared with the manual delineation of 2 experienced clinicians, and the best agreement was found with the threshold of 110%.

Patient-specific finite element models were constructed (Figure 1C). The 2-dimensional slices were axially stacked together, and axial smoothing was performed to reconstruct the 3-dimensional geometry. A volume curve-fitting technique was used by dividing the 3-dimensional domain into hundreds of small volumes to curve-fit the irregular geometry with component inclusions.[21] The entire structure was therefore meshed using hexahedron elements.

Because the configuration acquired in the CT images was pressurized, both circumferential and axial shrinkage was performed to determine the computational start shape.[22] Patient-specific blood pressure was used as the loading condition. Material properties of aneurysmal tissues were provided in Material in the Data Supplement. Numeric models were solved using ADINA 8.7 (ADINA R&D Inc). The von Mises stress was used as the quantitative indicator of the biomechanical environment (Figure 1C and 1F), with its top 5 percentile values being discarded to minimize the influence of mesh imperfection. For each patient, the stress was normalized by its peak value within the AAA wall to provide the mechanics-defined relative severity in the range of 0 to 1. Although both ILT and calcium were considered when mechanical analyses were performed, only stress in the wall was extracted for analysis because aneurysm rupture is the result of wall failure.

Image Coregistration and Octant-Based Data Sampling

The ^{18}F-FDG PET and contrast-enhanced CT images were resampled and coregistered (Figure 1) using rigid transformation to minimize the signal intensity difference of the vertebra in a custom platform written in MATLAB R2014a (The MathWorks, Inc), allowing measurement of the maximum aortic wall standardized uptake value (SUV_{max}). For precise matching of stress and PET data sets, each consecutive resampled axial slice throughout the length of the AAA (defined by max anteroposterior diameter >3.0 cm) was radially divided into 8 octants with area of 41.34 (30.07–72.46) mm^2 (interquartile range). The AAA neck was defined as the segment of aorta bordering the first slice of aneurysmal aorta (≈6.5 mm above and below the first >3.0 cm diameter slice), and the sac comprises the region between the aneurysm neck and the inferior aspect of the aneurysm. In addition to stress and ^{18}F-FDG SUV_{max} within the wall, ILT ratio and calcium ratio were also determined for each octant.

Statistical Analysis

All statistical analysis were performed in MATLAB, with statistical significance assumed if $P<0.05$. As the data were nested (8 octants within each slice and multiple slices for each AAA), linear mixed-effects models were used to appropriately account for the hierarchical data structure (details provided in Material in the Data Supplement). Both uni- and multivariate analyses were performed. Backward elimination, which started with more complicated linear mixed-effects models and removed the insignificant effects based on the Akaike information criterion, was used in the multivariate analysis. Moreover, to better quantify the contribution of structural stress, multivariate models without (the null model) and with (the full model) the consideration of stress were obtained and compared.

The power of each fixed effect was evaluated using the receiver-operating characteristic curve, and Youden criterion was used to identify the optimal operating point. To determine whether 2 sets of data differ significantly from each other, 2-tailed Student *t* test or Mann–Whitney test was used where appropriate.

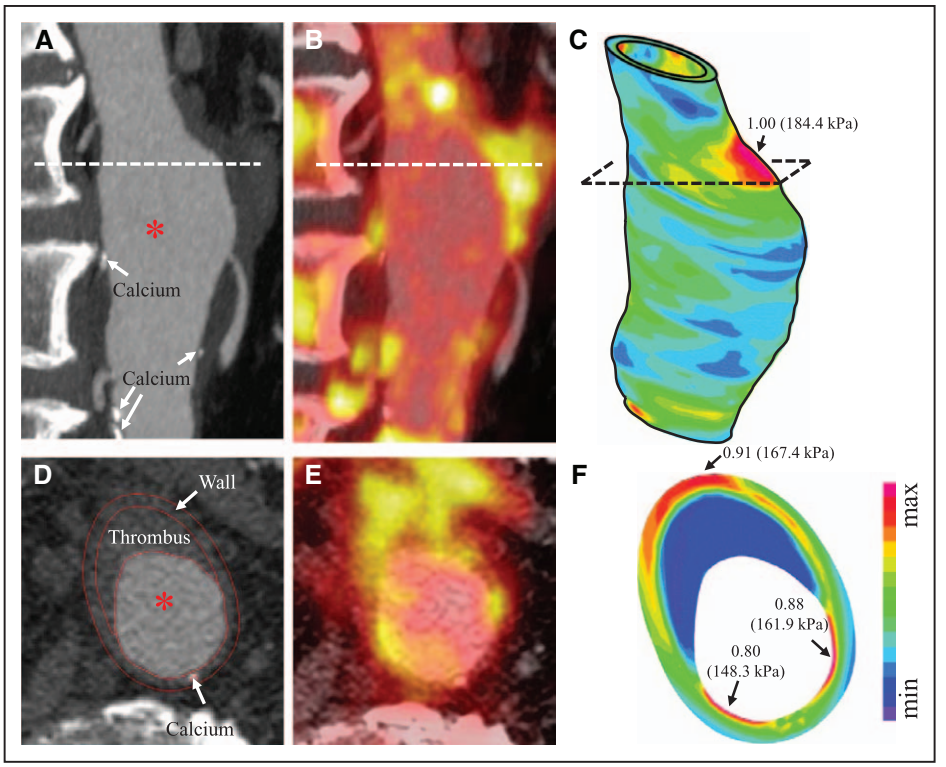

Figure 1. In vivo images and the calculated structural stress of an abdominal aortic aneurysm: (**A**) contrast-enhanced computed tomography (CT), sagittal view; (**B**) fluorine-18-labeled 2-deoxy-2-fluoro-D-glucose (^{18}F-FDG) positron emission tomography (PET), sagittal view; (**C**) structural stress plotted on the 3-dimensional geometry (both normalized and absolute values); (**D**) contrast-enhanced CT, transverse view; (**E**) ^{18}F-FDG PET, transverse view; and (**F**) structural stress plotted on the transverse plane (both normalized and absolute values).

Results

Clinical Demographics, AAA Morphology, and Composition

In total, 9192 octants were included in the analysis from 21 patients. Mean age was 78.4±6.7 years, and 19 of the 21 (90.5%) subjects were male. Six of the 21 patients (28.6%) had previous cardiovascular disease. Mean AAA size was 4.10±0.54 cm. More patient demographics and descriptions of each aneurysm can be found in Table 1.

Using the linear mixed-effects model, when results from all octants were pooled, slice outer wall diameter, ILT ratio, and calcium ratio were all found to be statistically significant predictors of ^{18}F-FDG uptake; in particular, SUV_{max} decreased with increasing ILT ratio (Figure 2A); whereas luminal diameter and patient demographic factors, including age, sex, body mass index, diabetes mellitus, and blood pressure, were not predictive (Table 2). To identify the hierarchical importance of these effective predictors, a multivariate linear mixed-effects analysis was performed (Table 3). Although statistically significant (P<0.0001), both local maximum wall diameter and calcium ratio had only a small effect on prediction of aortic SUV_{max}. ILT ratio had a larger effect on SUV_{max}, with each 10% increase in ILT area decreasing the SUV_{max} by 0.121 (P<0.0001) in the wall. This was confirmed by comparing the SUV_{max} in octants with and without ILT. Octants with thrombus demonstrated a lower SUV_{max} than the ILT-free octants (number of octants [number of patients]: 4475 (n=21) versus 4717 (n=21), SUV_{max}: 1.64 [1.27–1.95] versus 1.75 [1.51–1.99], P<0.0001; Figure 3). However, octants with ILT were associated with a larger SUV_{max} range than those without (with ILT: 0.40–2.94 versus without ILT: 0.77–2.72; Figure 3).

The random effects covariance parameters (psi) associated with octant number, anatomic location, and patient subjects are 0.012, 3.464×10^{-4}, and 0.025, respectively. This suggests,

Table 1. Characteristics of the Abdominal Aortic Aneurysm Subjects (n=21)

	Mean±SD, Median [IQR], or n (%)
Age, y	78.4±6.7
Sex (% male)	90 (19/21)
Body mass index, kg/m^2	26.0±2.5
Previous cardiovascular disease (% total)	29 (6/21)
Hypertension (% total)	19 (4/21)
Diabetes mellitus (% total)	5 (1/21)
Smoking (% total)	52 (11/21)
Statin (% total)	100 (21/21)
High-sensitivity C-reactive protein, mg/L	2.66±2.86
Total cholesterol, mmol/L	4.34±1.02
LDL cholesterol, mmol/L	2.28±0.86
Systolic blood pressure, mm Hg	137±21
Diastolic blood pressure, mm Hg	82±11
AAA baseline size, cm	4.10±0.54
SUV_{max} (median [IQR])	1.70 [1.41–1.98]
AAA ILT volume percentage, %	43 [18–49]
AAA Calcium volume percentage, %	3 [1–5]

AAA indicates abdominal aortic aneurysm; ILT, intraluminal thrombus; IQR, interquartile range; LDL, low-density lipoprotein; and SUV_{max}, maximum standardized uptake value.

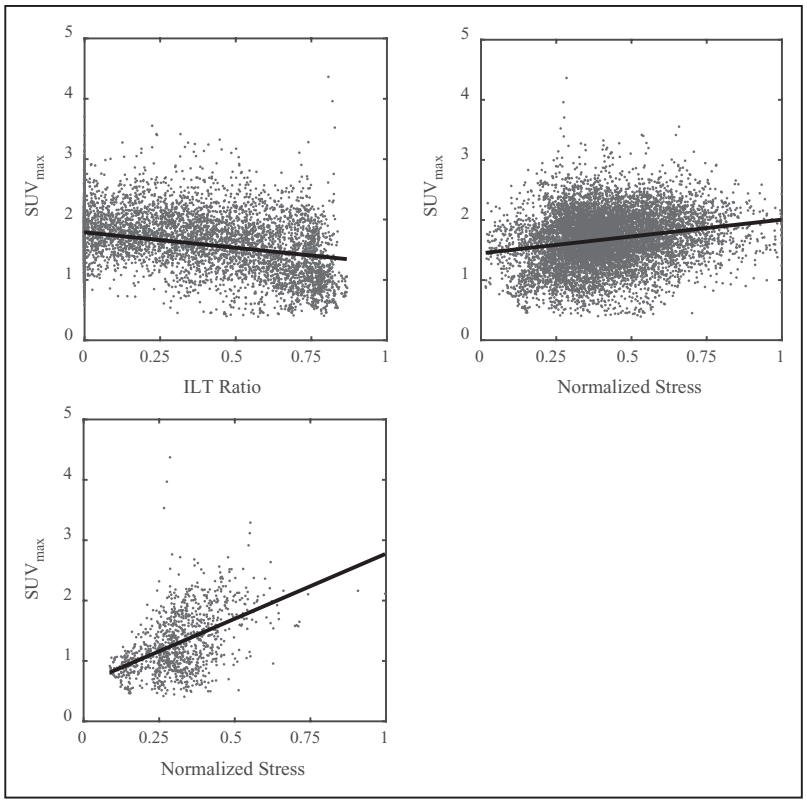

Figure 2. Scatter plot between the maximum standard uptake value (SUV_{max}) of fluorine-18-labeled 2-deoxy-2-fluoro-D-glucose positron emission tomography and morphological features or structural stress: (**A**) SUV_{max} vs intraluminal thrombus (ILT) ratio; (**B**) SUV_{max} vs normalized stress in all regions; and (**C**) SUV_{max} vs normalized stress in regions with ILT ratio >0.67.

for instance, a standard deviation of 0.158 (95% confidence level [0.116–0.215]) in SUV_{max} associated with the difference among individual patients. Such random effects arise from the hierarchical data structure that should be properly considered using mixed-effects models.

Table 2. Fixed Effects Coefficients of the Univariate Linear Mixed Effects Analysis With Respect to SUV_{max}

Fixed Effects	Estimate	Standard Error	*P* Value
Age, y	−0.002	0.006	0.770
Sex (male=1; female=0)	0.043	0.132	0.746
Body mass index, kg/m^2	−0.004	0.016	0.812
Diabetes mellitus	−0.216	0.176	0.221
Hypertension	−0.107	0.096	0.268
Previous cardiovascular disease	0.110	0.083	0.183
Smoking	−0.029	0.078	0.707
Total cholesterol, mmol/L	0.022	0.039	0.565
Systolic blood pressure, mm Hg	−0.002	0.002	0.271
Diastolic blood pressure, mm Hg	−0.004	0.003	0.236
Slice luminal diameter, cm	0.009	0.009	0.330
Slice outer wall diameter, cm	−0.046	0.007	<0.0001
ILT ratio	−0.553	0.016	<0.0001
Calcium ratio	0.220	0.046	<0.0001
Normalized stress	0.552	0.031	<0.0001

The units of fixed effects were shown in the first column, and those not provided were dimensionless. ILT indicates intraluminal thrombus; and SUV_{max}, maximum standardized uptake value.

Structural Stress Versus ^{18}F-FDG Uptake

When comparing normalized stress and SUV_{max} in all wall regions using the univariate linear mixed-effects model, a positive correlation was observed with a slope estimate of 0.552 (P<0.0001; Table 2; Figure 2B). An enhanced relationship was observed in octants with ILT occupying >67% of the area (Figure 2C). This impact of ILT content was confirmed by multivariate linear mixed-effects analysis. In the multivariate model, although normalized stress itself did not demonstrate any statistical significance in the prediction of SUV_{max}, the interaction between normalized stress and ILT ratio leads to an increase in SUV_{max} (P<0.0001; Table 3 and Figure 4).

Table 3. Fixed Effects Coefficients of the Full Linear Mixed Effects Model of SUV_{max}

Fixed Effects	Estimate	Standard Error	*P* Value
Intercept, g/mL	1.540	0.064	<0.0001
Prior cardiovascular disease	0.190	0.077	0.013
Slice outer wall diameter, cm	0.057	0.007	<0.0001
ILT ratio	−1.209	0.042	<0.0001
Calcium ratio	−0.138	0.046	0.003
Normalized stress	0.019	0.034	0.58
Stress-ILT interaction	1.688	0.102	<0.0001

The intercept had same unit as SUV_{max}, previous cardiovascular disease was categorical, slice outer diameter was measured in centimeters, and all other predictors were dimensionless in the range of 0 to 1. ILT indicates intraluminal thrombus; and SUV_{max}, maximum standardized uptake value.

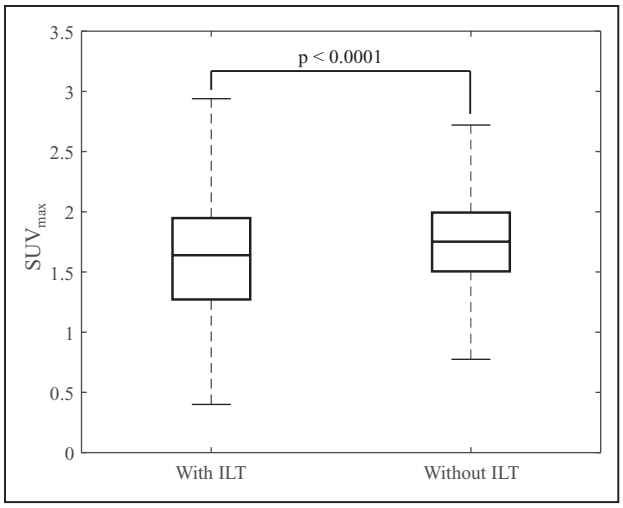

Figure 3. Comparison of maximum standardized uptake value (SUV_{max}) in regions with and without local intraluminal thrombus (ILT).

The Incremental Value of Structural Stress in Defining High ^{18}F-FDG Uptake

Multivariate linear mixed-effects analysis was performed both with and without the inclusion of stress. Compared with the model without considering stress, the full linear mixed-effects model lead to a reduction of Akaike information criterion value by 344.3. This indicated that stress was an important effect and should not be neglected. Therefore, results reported for the multivariate analysis were based on the model with stress.

Receiver-operating characteristic curve analysis was performed to identify factors that might help predict octants with high (SUV_{max}>2) and low (SUV_{max}≤2) ^{18}F-FDG uptake[23] and to determine the optimal threshold for stress in relation to ^{18}F-FDG uptake. Normalized stress (AUC=0.59; Area Under the Curve) was a better predictor of ^{18}F-FDG uptake when compared with morphological features, including maximum outer diameter (AUC=0.49), ILT ratio (AUC=0.55), and calcium ratio (AUC=0.52; Figure 5). AUC of stress increased from 0.59 to 0.66 when limited to octants with ILT ratio >0.33 (n=2894 from 20 patients). For octants with ILT ratio >0.67 (n=1064 from 16 patients), the AUC of stress further rose to 0.80. In this subset, the optimal operating point for the differentiation of SUV_{max} was identified as a normalized stress of 0.45. When using a 0.45 stress threshold to determine high and low stress among 1064 octants with ILT ratio >0.67, higher ^{18}F-FDG uptake was found in the high stress group (median [interquartile range]: 1.93 [1.60–2.14] versus 1.14 [0.90–1.53]; *P*<0.0001; Figure 6).

Discussion

In this study, we explored relationships between wall structural stress, AAA morphology and compositions, and inflammation determined by ^{18}F-FDG PET. In the case of aneurysm wall, there is reasonable evidence that FDG preferentially accumulates in inflamed areas.[5,10,24] We observed a link between stress and inflammation, particularly in aneurysmal regions with high ILT. To the best of our knowledge, this is the first retrospective clinical study to quantify the effect of AAA morphology and composition with regard to wall stress and inflammation.

ILT plays a pivotal role in the pathogenesis of AAA, with both potentially protective and deleterious effects. Although ILT seems in part to protect against AAA rupture through a cushioning effect that reduces wall stress,[25,26] it also weakens the vessel wall, increasing rate of AAA expansion.[27] Our findings

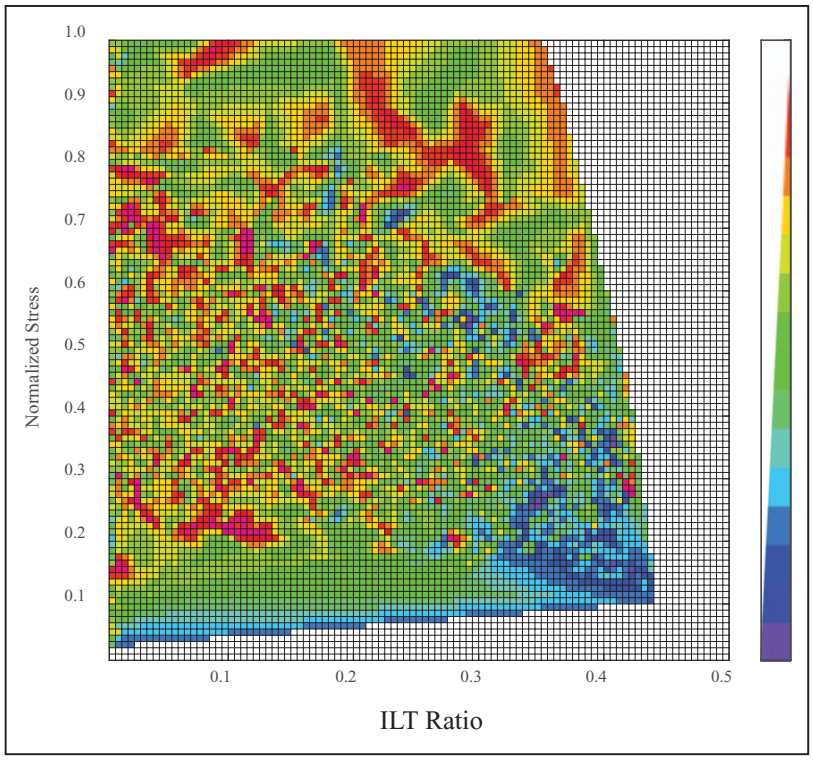

Figure 4. Heat map showing the relation between maximum standardized uptake value (SUV_{max}), intraluminal thrombus (ILT) ratio, and normalized stress. The value of SUV_{max} is indicated by the color of each grid.

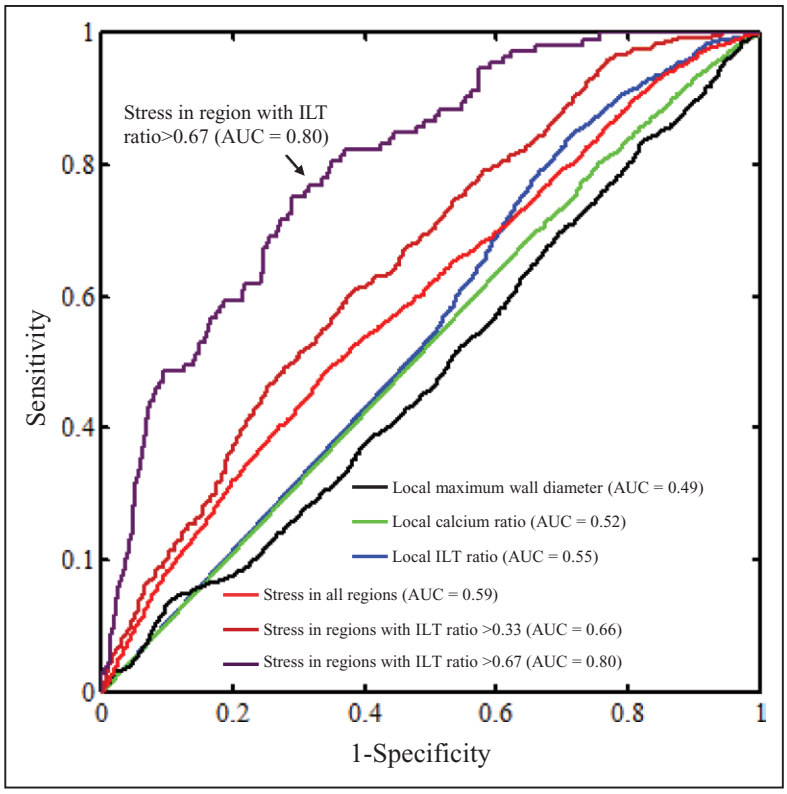

Figure 5. Serial receiver-operating characteristic curve analyses comparing the capability of differentiating regions with high (maximum standardized uptake value [SUV_{max}]>2) and low (SUV_{max}≤2) fluorine-18-labeled 2-deoxy-2-fluoro-D-glucose uptake. The structural stress lead to an improved prediction compared with abdominal aortic aneurysm morphology and composition, and this further improved with the combination of the extent of local intraluminal thrombus (ILT). AUC indicates area under the curve.

mirror this dichotomy. Overall, there was a negative correlation between ILT ratio and SUV_{max} (Figure 2A), which is possibly explained by lower wall stress because of increased ILT area (Figure 7). We observed increased ^{18}F-FDG uptake in relation to harsh mechanical conditions in the aortic wall beneath a thick ILT. This finding is supported by previous studies showing increased inflammatory infiltration in AAA wall beneath ILT.[28] Heavy ILT burden might also lead to local hypoxia and neovascularization,[29] which could, in principle, augment cellular ^{18}F-FDG uptake.[30] A causal relationship between high structural stress and AAA inflammation has previously been suggested.[12] At the cellular level, among other pathogenic mechanisms, high stress increases reactive oxygen species production within vascular smooth muscle cells, which activates nuclear factor-kappa B[31] and promotes inflammation.[32] Mechanical loading might also cause enhanced proteolytic activities in macrophages.[33]

Aneurysm is a multicomponent inhomogeneous structure with irregular geometry. Its components and geometric determinants undoubtedly influence the mechanical environment within the structure[25,34] (Figure I in the Data Supplement). If calcium and ILT were treated as wall, the stress distribution changed dramatically (Figure II in the Data Supplement). The multivariate analysis in this study showed that compared with local luminal and outer wall diameter, both percentage ILT and calcium had a greater influence in stress calculation. Although in general, stress within the structure decreased as ILT increased (Figure 6), as shown in Figure IA in the Data Supplement, high stress areas are still found in regions with a high ILT ratio. This study also showed that in addition to ILT, calcium ratio was associated with ^{18}F-FDG uptake negatively although the effect was weak (Table 3). It may be because of the ability of calcium in undertaking mechanical loading increases with its size. As a result, stress in AAA wall decreased while calcium ratio increases (Figure IB in the Data Supplement).

In this study, modeled scatter correction is applied by the GE Discovery 690 PET/CT scanner, which should limit the degrading impact of scatter. The scanner uses a relatively narrow energy window (425–650 keV) to limit scattered coincidences, in combination with modeled scatter correction as part of the image reconstruction algorithm that includes compensation for multiple scattered events and single scatter events. The partial volume effect resulting from limited spatial resolution, however, is a limitation of this study that may affect FDG value

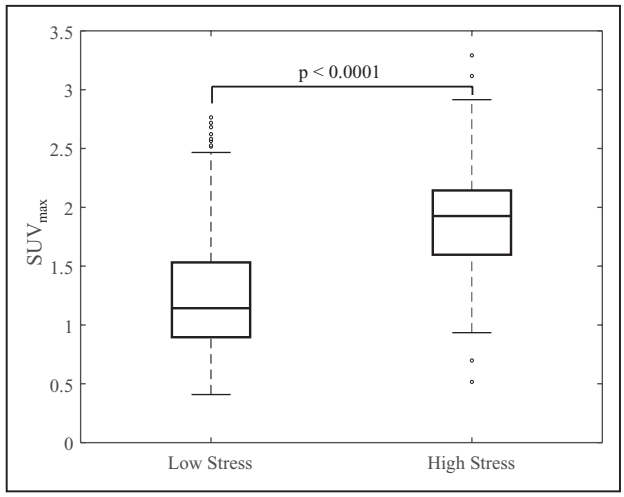

Figure 6. Comparison of maximum standardized uptake value (SUV_{max}) in regions with low (≤0.45) and high (>0.45) structural stress. This comparison was performed in the regions with intraluminal thrombus (ILT) ratio >0.67, and the stress threshold was identified earlier in the receiver-operating characteristic curve analyses.

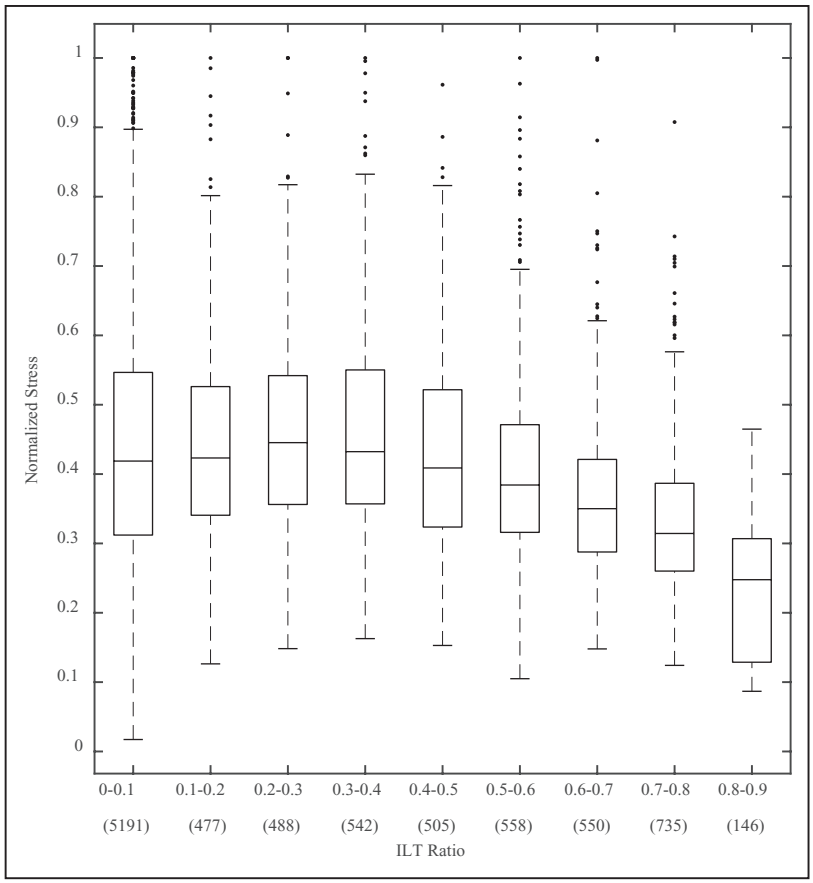

Figure 7. Relation between normalized stress and local intraluminal thrombus (ILT) ratio within each octant (the figure in the brackets blow the *x* axis showed the number of octants).

used for analysis; ^{18}F-FDG PET signals relating to the aneurysm wall might reflect some spillover from nearby structures, such as ILT, in addition to true aortic wall uptake. To assess the partial volume effect on the results of the present study, we increased the wall thickness inward by 1 pixel (≈0.6 mm), re-extracted the SUV_{max} within the wall and compared with our original results. SUV_{max} in these 2 scenarios remained highly consistent; the difference was <1% when comparing all octants (original wall thickness: 1.70 [1.41–1.98] versus increased wall thickness 1.71 [1.42–1.98]) and <2% when comparing octants with ILT ratio >0.67 (1.20 [0.93–1.65] versus 1.22 [0.94–1.66]). We therefore concluded that partial volume effect was associated with little impact onto the quantitative results in this study. Such an observation could be explained by the spatial distribution of inflammatory infiltration in the ILT. Previous studies using immunohistochemical analysis[35,36] and flow cytometry[37] have shown that the extent of inflammatory cell infiltration decreases significantly with increasing distance to lumen, for example, the average percentage of macrophages measured 8 mm from the vessel lumen reduced to ≈3%, compared with significantly higher percentage at the luminal surface.[35] Therefore, although signal spillover from ILT might contribute to ^{18}F-FDG AAA wall signal intensity, it is likely that the highest inflammatory signals originating from ILT occur close to the lumen where they are less likely to significantly influence the signal within AAA wall providing ILT is thick.

One of the key findings in the present study is that the combination of stress and local ILT burden, rather than either factor alone, could lead to better prediction of increased ^{18}F-FDG uptake in AAA wall. The interaction term in the linear mixed effect model suggests that the role of mechanical stress becomes increasingly important with greater ILT ratio, which is also shown in the receiver-operating characteristic curve analysis where AUC improved when the analysis was limited to regions with thick ILT. Mechanics showed relatively poorer predictive power in regions with no or thin thrombus, which could potentially be explained by several factors: (1) further morphological stratification of these regions may be needed to differentiate, for example, an octant with little ILT formation versus an octant from AAA with heavy ILT burden arising at the so-called shoulder area that lacks thrombus but where inflammation remains high; and (2) in octants with less ILT, the partial volume effect might be more likely to influence apparent ^{18}F-FDG uptake within the wall than in octants with thick ILT as described above. The main clinical benefit from our findings would be the ability to identify a subgroup of patients with small AAAs but high FDG uptake, ILT load, and mechanical stress. These aneurysms may experience more rapid expansion than average, requiring more frequent surveillance and prophylactic repair before rupture. However, further longitudinal studies, with clinical outcomes, are warranted to determine the clinical significance of these findings.

Overall, our results are consistent with previous studies comparing finite element analysis-derived structural stress and ^{18}F-FDG PET. In one study, Xu et al[17] compared the ^{18}F-FDG uptake and structural stress in 5 patients with aneurysms in the descending thoracic or abdominal aorta. Using a visual comparison, authors reported that high structural stress

regions colocalized with areas of elevated ^{18}F-FDG uptake. Furthermore, both high structural stress and increased ^{18}F-FDG uptake occurred at the site of future rupture in 2 cases. In another study, Maier et al[18] showed a positive correlation (r=0.71; P=0.0005) between ^{18}F-FDG uptake and structural stress, including 18 patients with AAA. Moreover, the ^{18}F-FDG uptake was resampled and mapped to the finite element geometry and significant element-wise correlation between structural stress and ^{18}F-FDG uptake was seen in 16 of 18 AAAs. In the largest study to date, Nchimi et al[19] investigated 53 patients with either infrarenal or thoracic aortic aneurysms, and a modest correlation between AAA stress and inflammation quantified by ^{18}F-FDG uptake was found using multivariate linear regression (r=0.26; P=0.0009). Our study not only confirmed these findings but also showed the potential of using structural stress, in combination with AAA composition, to differentiate the low/high ^{18}F-FDG uptake regions.

The present study has several limitations and assumptions. First, although each patient underwent a contrast-enhanced CT aortogram, inherent limitations of CT imaging sometimes made delineation of the aortic outer wall boundary difficult. Despite our best efforts to accurately delineate the structural components during the segmentation process, it was not always possible to define the exact border between AAA wall and ILT. We therefore assumed a uniform wall thickness for our calculations. In reality, AAA wall thickness will vary depending on multiple factors,[38] such as ILT burden[28] and spatial location.[39,40] A sensitivity analysis with models of both uniform and variable wall thickness was performed. Stresses calculated from both models showed excellent correlation (Figures II and III in the Data Supplement). Therefore, we are confident that the limitations of our border delineation did not have a material effect on overall results. Second, limited CT tissue contrast also precluded the use of an anatomic-based PET partial volume correction in our analysis. This may be possible as PET/magnetic resonance imaging becomes more available. Third, no side branches were considered for stress modeling. Fourth, piecewise homogeneous, isotropic material was used for the simulations, and the influence of fiber orientation was not accounted for. Finally, the computational models were structure-only, and effects because of blood flow were not considered. However, 3-dimensional structure-only analysis is computationally inexpensive and can provide accurate results.[41]

Conclusion

Increased inflammation depicted by ^{18}F-FDG was observed in AAA wall regions subjected to high mechanical stresses, especially in the presence of significant ILT. Because of the complicated 3-dimensional structure of AAA, the cushioning effect of ILT might be ineffective in certain circumstances, resulting in a combination of high stress and weakened aortic wall in the presence of ILT that might accelerate inflammation and other pathogenic processes in AAA. The present study provides a mechanistic insight into the relationship between structural stress and inflammation.

Acknowledgments

We thank Dr Shahin Tavakoli and Mr Tengyao Wang from the Statistical Laboratory, Department of Pure Mathematics and Mathematical Statistics, University of Cambridge, for the assistance in statistical analyses.

Sources of Funding

This study was supported by the British Heart Foundation Cambridge Centre of Excellence (RE/13/6/30180), Heart Research UK (RG2638/14/16), EPSRC Centre for Mathematical and Statistical Analysis of Multimodal Clinical Imaging (EP/N014588/1), and the National Institute for Health Research (NIHR) Cambridge Biomedical Research Centre. Dr Tarkin is supported by a Wellcome Trust research training fellowship (104492/Z/14/Z). Dr Rudd is part-supported by the NIHR Cambridge Biomedical Research Centre, the British Heart Foundation, the Wellcome Trust, and Higher Education Funding Council for England (HEFCE). Dr Newby is supported by the British Heart Foundation (CH/09/002) and is the recipient of a Wellcome Trust Senior Investigator Award (WT103782AIA).

Disclosures

None.

References

1. Kent KC. Clinical practice. Abdominal aortic aneurysms. *N Engl J Med*. 2014;371:2101–2108. doi: 10.1056/NEJMcp1401430.
2. Ashton HA, Buxton MJ, Day NE, Kim LG, Marteau TM, Scott RA, Thompson SG, Walker NM; Multicentre Aneurysm Screening Study Group. The Multicentre Aneurysm Screening Study (MASS) into the effect of abdominal aortic aneurysm screening on mortality in men: a randomised controlled trial. *Lancet*. 2002;360:1531–1539.
3. Powell JT, Brown LC, Greenhalgh RM, Thompson SG. The rupture rate of large abdominal aortic aneurysms: is this modified by anatomical suitability for endovascular repair? *Ann Surg*. 2008;247:173–179. doi: 10.1097/SLA.0b013e3181557d2a.
4. Shah PK. Inflammation, metalloproteinases, and increased proteolysis: an emerging pathophysiological paradigm in aortic aneurysm. *Circulation*. 1997;96:2115–2117.
5. Courtois A, Nusgens BV, Hustinx R, Namur G, Gomez P, Somja J, Defraigne JO, Delvenne P, Michel JB, Colige AC, Sakalihasan N. 18F-FDG uptake assessed by PET/CT in abdominal aortic aneurysms is associated with cellular and molecular alterations prefacing wall deterioration and rupture. *J Nucl Med*. 2013;54:1740–1747. doi: 10.2967/jnumed.112.115873.
6. Wilson WR, Anderton M, Schwalbe EC, Jones JL, Furness PN, Bell PR, Thompson MM. Matrix metalloproteinase-8 and -9 are increased at the site of abdominal aortic aneurysm rupture. *Circulation*. 2006;113:438–445. doi: 10.1161/CIRCULATIONAHA.105.551572.
7. Henderson EL, Geng YJ, Sukhova GK, Whittemore AD, Knox J, Libby P. Death of smooth muscle cells and expression of mediators of apoptosis by T lymphocytes in human abdominal aortic aneurysms. *Circulation*. 1999;99:96–104.
8. Shimizu K, Mitchell RN, Libby P. Inflammation and cellular immune responses in abdominal aortic aneurysms. *Arterioscler Thromb Vasc Biol*. 2006;26:987–994. doi: 10.1161/01.ATV.0000214999.12921.4f.
9. Hellenthal FA, Buurman WA, Wodzig WK, Schurink GW. Biomarkers of abdominal aortic aneurysm progression. Part 2: inflammation. *Nat Rev Cardiol*. 2009;6:543–552. doi: 10.1038/nrcardio.2009.102.
10. Reeps C, Essler M, Pelisek J, Seidl S, Eckstein HH, Krause BJ. Increased 18F-fluorodeoxyglucose uptake in abdominal aortic aneurysms in positron emission/computed tomography is associated with inflammation, aortic wall instability, and acute symptoms. *J Vasc Surg*. 2008;48:417–423; discussion 424. doi: 10.1016/j.jvs.2008.03.059.
11. Sakalihasan N, Van Damme H, Gomez P, Rigo P, Lapiere CM, Nusgens B, Limet R. Positron emission tomography (PET) evaluation of abdominal aortic aneurysm (AAA). *Eur J Vasc Endovasc Surg*. 2002;23:431–436. doi: 10.1053/ejvs.2002.1646.
12. Qiu J, Zheng Y, Hu J, Liao D, Gregersen H, Deng X, Fan Y, Wang G. Biomechanical regulation of vascular smooth muscle cell functions: from *in vitro* to *in vivo* understanding. *J R Soc Interface*. 2014;11:20130852. doi: 10.1098/rsif.2013.0852.
13. Grote K, Flach I, Luchtefeld M, Akin E, Holland SM, Drexler H, Schieffer B. Mechanical stretch enhances mRNA expression and proenzyme release of matrix metalloproteinase-2 (MMP-2) via NAD(P)H oxidase-derived

reactive oxygen species. *Circ Res*. 2003;92:e80–e86. doi: 10.1161/01.RES.0000077044.60138.7C.
14. Fillinger MF, Marra SP, Raghavan ML, Kennedy FE. Prediction of rupture risk in abdominal aortic aneurysm during observation: wall stress versus diameter. *J Vasc Surg*. 2003;37:724–732. doi: 10.1067/mva.2003.213.
15. Erhart P, Hyhlik-Dürr A, Geisbüsch P, Kotelis D, Müller-Eschner M, Gasser TC, von Tengg-Kobligk H, Böckler D. Finite element analysis in asymptomatic, symptomatic, and ruptured abdominal aortic aneurysms: in search of new rupture risk predictors. *Eur J Vasc Endovasc Surg*. 2015;49:239–245. doi: 10.1016/j.ejvs.2014.11.010.
16. Hyhlik-Dürr A, Krieger T, Geisbüsch P, Kotelis D, Able T, Böckler D. Reproducibility of deriving parameters of AAA rupture risk from patient-specific 3D finite element models. *J Endovasc Ther*. 2011;18:289–298. doi: 10.1583/10-3384MR.1.
17. Xu XY, Borghi A, Nchimi A, Leung J, Gomez P, Cheng Z, Defraigne JO, Sakalihasan N. High levels of 18F-FDG uptake in aortic aneurysm wall are associated with high wall stress. *Eur J Vasc Endovasc Surg*. 2010;39:295–301. doi: 10.1016/j.ejvs.2009.10.016.
18. Maier A, Essler M, Gee MW, Eckstein HH, Wall WA, Reeps C. Correlation of biomechanics to tissue reaction in aortic aneurysms assessed by finite elements and [18F]-fluorodeoxyglucose-PET/CT. *Int J Numer Method Biomed Eng*. 2012;28:456–471. doi: 10.1002/cnm.1477.
19. Nchimi A, Cheramy-Bien JP, Gasser TC, Namur G, Gomez P, Seidel L, Albert A, Defraigne JO, Labropoulos N, Sakalihasan N. Multifactorial relationship between 18F-fluoro-deoxy-glucose positron emission tomography signaling and biomechanical properties in unruptured aortic aneurysms. *Circ Cardiovasc Imaging*. 2014;7:82–91. doi: 10.1161/CIRCIMAGING.112.000415.
20. Bischoff B, Kantert C, Meyer T, Hadamitzky M, Martinoff S, Schömig A, Hausleiter J. Cardiovascular risk assessment based on the quantification of coronary calcium in contrast-enhanced coronary computed tomography angiography. *Eur Heart J Cardiovasc Imaging*. 2012;13:468–475. doi: 10.1093/ejechocard/jer261.
21. Tang D, Yang C, Kobayashi S, Zheng J, Woodard PK, Teng Z, Billiar K, Bach R, Ku DN. 3D MRI-based anisotropic FSI models with cyclic bending for human coronary atherosclerotic plaque mechanical analysis. *J Biomech Eng*. 2009;131:061010. doi: 10.1115/1.3127253.
22. Tang D, Teng Z, Canton G, Hatsukami TS, Dong L, Huang X, Yuan C. Local critical stress correlates better than global maximum stress with plaque morphological features linked to atherosclerotic plaque vulnerability: an *in vivo* multi-patient study. *Biomed Eng Online*. 2009;8:15. doi: 10.1186/1475-925X-8-15.
23. Truijers M, Kurvers HA, Bredie SJ, Oyen WJ, Blankensteijn JD. *In vivo* imaging of abdominal aortic aneurysms: increased FDG uptake suggests inflammation in the aneurysm wall. *J Endovasc Ther*. 2008;15:462–467. doi: 10.1583/08-2447.1.
24. Courtois A, Nusgens BV, Hustinx R, Namur G, Gomez P, Kuivaniemi H, Defraigne JO, Colige AC, Sakalihasan N. Gene expression study in positron emission tomography-positive abdominal aortic aneurysms identifies CCL18 as a potential biomarker for rupture risk. *Mol Med*. 2015;20:697–706. doi: 10.2119/molmed.2014.00065.
25. Li ZY, U-King-Im J, Tang TY, Soh E, See TC, Gillard JH. Impact of calcification and intraluminal thrombus on the computed wall stresses of abdominal aortic aneurysm. *J Vasc Surg*. 2008;47:928–935. doi: 10.1016/j.jvs.2008.01.006.
26. Wang DH, Makaroun MS, Webster MW, Vorp DA. Effect of intraluminal thrombus on wall stress in patient-specific models of abdominal aortic aneurysm. *J Vasc Surg*. 2002;36:598–604.
27. Nchimi A, Courtois A, El Hachemi M, Touat Z, Drion P, Withofs N, Warnock G, Bahri MA, Dogné JM, Cheramy-Bien JP, Schoysman L, Joskin J, Michel JB, Defraigne JO, Plenevaux A, Sakalihasan N. Multimodality imaging assessment of the deleterious role of the intraluminal thrombus on the growth of abdominal aortic aneurysm in a rat model. *Eur Radiol*. 2016;26:2378–2386. doi: 10.1007/s00330-015-4010-y.
28. Kazi M, Thyberg J, Religa P, Roy J, Eriksson P, Hedin U, Swedenborg J. Influence of intraluminal thrombus on structural and cellular composition of abdominal aortic aneurysm wall. *J Vasc Surg*. 2003;38:1283–1292. doi: 10.1016/S0741.
29. Vorp DA, Lee PC, Wang DH, Makaroun MS, Nemoto EM, Ogawa S, Webster MW. Association of intraluminal thrombus in abdominal aortic aneurysm with local hypoxia and wall weakening. *J Vasc Surg*. 2001;34:291–299. doi: 10.1067/mva.2001.114813.
30. Tarkin JM, Joshi FR, Rudd JH. PET imaging of inflammation in atherosclerosis. *Nat Rev Cardiol*. 2014;11:443–457. doi: 10.1038/nrcardio.2014.80.
31. Hishikawa K, Oemar BS, Yang Z, Lüscher TF. Pulsatile stretch stimulates superoxide production and activates nuclear factor-kappa B in human coronary smooth muscle. *Circ Res*. 1997;81:797–803.
32. McCormick ML, Gavrila D, Weintraub NL. Role of oxidative stress in the pathogenesis of abdominal aortic aneurysms. *Arterioscler Thromb Vasc Biol*. 2007;27:461–469. doi: 10.1161/01.ATV.0000257552.94483.14.
33. Yang JH, Sakamoto H, Xu EC, Lee RT. Biomechanical regulation of human monocyte/macrophage molecular function. *Am J Pathol*. 2000;156:1797–1804. doi: 10.1016/S0002-9440(10)65051-1.
34. Maier A, Gee MW, Reeps C, Eckstein HH, Wall WA. Impact of calcifications on patient-specific wall stress analysis of abdominal aortic aneurysms. *Biomech Model Mechanobiol*. 2010;9:511–521. doi: 10.1007/s10237-010-0191-0.
35. Adolph R, Vorp DA, Steed DL, Webster MW, Kameneva MV, Watkins SC. Cellular content and permeability of intraluminal thrombus in abdominal aortic aneurysm. *J Vasc Surg*. 1997;25:916–926.
36. Folkesson M, Silveira A, Eriksson P, Swedenborg J. Protease activity in the multi-layered intra-luminal thrombus of abdominal aortic aneurysms. *Atherosclerosis*. 2011;218:294–299. doi: 10.1016/j.atherosclerosis.2011.05.002.
37. Sagan A, Mrowiecki W, Mikolajczyk TP, Urbanski K, Siedlinski M, Nosalski R, Korbut R, Guzik TJ. Local inflammation is associated with aortic thrombus formation in abdominal aortic aneurysms. Relationship to clinical risk factors. *Thromb Haemost*. 2012;108:812–823. doi: 10.1160/TH12-05-0339.
38. Raut SS, Jana A, De Oliveira V, Muluk SC, Finol EA. The importance of patient-specific regionally varying wall thickness in abdominal aortic aneurysm biomechanics. *J Biomech Eng*. 2013;135:81010. doi: 10.1115/1.4024578.
39. Thubrikar MJ, Labrosse M, Robicsek F, Al-Soudi J, Fowler B. Mechanical properties of abdominal aortic aneurysm wall. *J Med Eng Technol*. 2001;25:133–142.
40. Raghavan ML, Kratzberg J, Castro de Tolosa EM, Hanaoka MM, Walker P, da Silva ES. Regional distribution of wall thickness and failure properties of human abdominal aortic aneurysm. *J Biomech*. 2006;39:3010–3016. doi: 10.1016/j.jbiomech.2005.10.021.
41. Huang Y, Teng Z, Sadat U, Graves MJ, Bennett MR, Gillard JH. The influence of computational strategy on prediction of mechanical stress in carotid atherosclerotic plaques: comparison of 2D structure-only, 3D structure-only, one-way and fully coupled fluid-structure interaction analyses. *J Biomech*. 2014;47:1465–1471. doi: 10.1016/j.jbiomech.2014.01.030.

CLINICAL PERSPECTIVE

Inflammation burden in the aortic abdominal aneurysm structure has been shown to be associated with patient clinical presentations, subsequent lesion progression, and deadly rupture. This study quantified the association between local ^{18}F-FDG uptake and structural stress in aortic abdominal aneurysm, lesion morphology, and compositions, including intraluminal thrombus and calcium. The coinfluence of structural stress and aneurysm architectural features on ^{18}F-FDG uptake-defined wall inflammation was demonstrated, suggesting a novel mechanistic link underlying aneurysm inflammation. This finding might enable the ability to identify a subgroup of patients with small aortic abdominal aneurysms but high FDG uptake, intraluminal thrombus load, and mechanical stress. These aneurysms might experience more aggressive disease development than average, requiring more frequent surveillance and prophylactic repair before rupture. Further longitudinal studies, with clinical outcomes, are warranted to determine the clinical significance of this finding.

Circulation
Cardiovascular Imaging

High Structural Stress and Presence of Intraluminal Thrombus Predict Abdominal Aortic Aneurysm ^{18}F-FDG Uptake: Insights From Biomechanics

Yuan Huang, Zhongzhao Teng, Maysoon Elkhawad, Jason M. Tarkin, Nikhil Joshi, Jonathan R. Boyle, John R. Buscombe, Timothy D. Fryer, Yongxue Zhang, Ah Yeon Park, Ian B. Wilkinson, David E. Newby, Jonathan H. Gillard and James H. F. Rudd

Circ Cardiovasc Imaging. 2016;9:
doi: 10.1161/CIRCIMAGING.116.004656
Circulation: Cardiovascular Imaging is published by the American Heart Association, 7272 Greenville Avenue, Dallas, TX 75231

Print ISSN: 1941-9651. Online ISSN: 1942-0080

Supplemental Material

Supplement to: Huang Y, Teng Z, Elkhawad M et al. High Structural Stress and Presence of Intraluminal Thrombus Predict Abdominal Aortic Aneurysm ^{18}F-FDG Uptake: Insights from Biomechanics

PET-CT Imaging Protocol

Patients fasted for at least 6 hours prior to imaging, consistent with established vascular PET imaging protocols[1]. A target activity of 240 MBq ^{18}F-FDG was injected intravenously after which patients rested in a quiet environment for 90 minutes before being transferred onto the PET/CT scanner. A low dose CT was performed for attenuation correction, followed by a PET scan covering three bed positions from the arch of aorta to the aortic bifurcation over 30 minutes (10 minutes per bed position). Tracer circulation times were based on previous studies using ^{18}F-FDG in atherosclerosis[2], aimed to produce optimal contrast between the aortic wall and the blood pool. With the patient lying in the same position, a CT aortogram from the diaphragm to the aortic bifurcation was performed using 75-100 mL of iodinated contrast (400 mgI/mL; Iomeron, Bracco, Milan, Italy), followed by 50 mL of 0.9% saline flush. PET data were reconstructed using the time of flight ordered subsets expectation-maximization (TOF-OSEM) algorithm implemented on the scanner, which incorporated the following data corrections: dead time, random coincidences, normalization, scatter, attenuation, sensitivity and radioactive decay.

Material properties of aneurysmal tissues

Tissues, including wall, ILT and calcium, were assumed to be hyperelastic, homogeneous, isotropic and incompressible with material properties described by the modified Mooney-Rivlin formulation:

$$W = c_1(\bar{I}_1 - 3) + D_1\left[exp\left(D_2(\bar{I}_1 - 3)\right) - 1\right] + \kappa(J - 1),$$

where $\bar{I}_1 = J^{-2/3}I_1$ and $J = det(\boldsymbol{F})$, $\boldsymbol{F}$ is the deformation gradient and I_1 is the first invariant of deformation tensor. κ is Lagrangian multiplier for the incompressibility. c_1, D_1, and D_2 are material parameters derived from previous experimental studies: arterial wall, c_1=0.07 kPa,

D_1=6.54 kPa, D_2=5.88; ILT, c_1=0.24 kPa, D_1=8.69 kPa, D_2=0.61; and calcium, c_1=7.24x10^3 kPa, D_1=0.01 kPa, D_2=2.34x10^{-14} [3-5].

Construction of linear mixed-effect models

Fixed-effect predictors included in the statistical model were: (I) clinical demographics and risk factors (age, gender, body-mass index, diabetes mellitus, blood pressure, prior cardiovascular events and smoking); (II) morphological measurements (slice luminal diameter, slice outer wall diameter, ILT ratio and calcium ratio); and (III) structural stress. Octant number, anatomical location (neck or sac) and patient subject were modeled as the random effects.

Compositional and geometrical features effecting the stress in the AAA wall

The deformation of each aneurysmal component was governed by the Cauchy momentum equation,

$$\rho_s \ddot{\boldsymbol{U}} = \nabla \cdot \boldsymbol{\sigma}$$

where $\boldsymbol{U}$ is the displacement vector, $\boldsymbol{\sigma}$ is the stress tensor and ρ_s is the density of each component. In the case of big deformation, the governing equation is non-linear. Moreover, the material property of each component is non-linear[3] and the geometry of each component is irregular. These factors interact with each other non-linearly, effecting the mechanical condition within the aneurysm structure. As shown in Figure S1 below, local luminal, outer wall diameter, ILT and calcium all significantly affected stress in the aneurysm, but the latter two had greater effects. It is worthwhile pointing out that although in general stress decreases when ILT increases (Figure S1A), the stress varies widely in regions with a large ILT ratio.

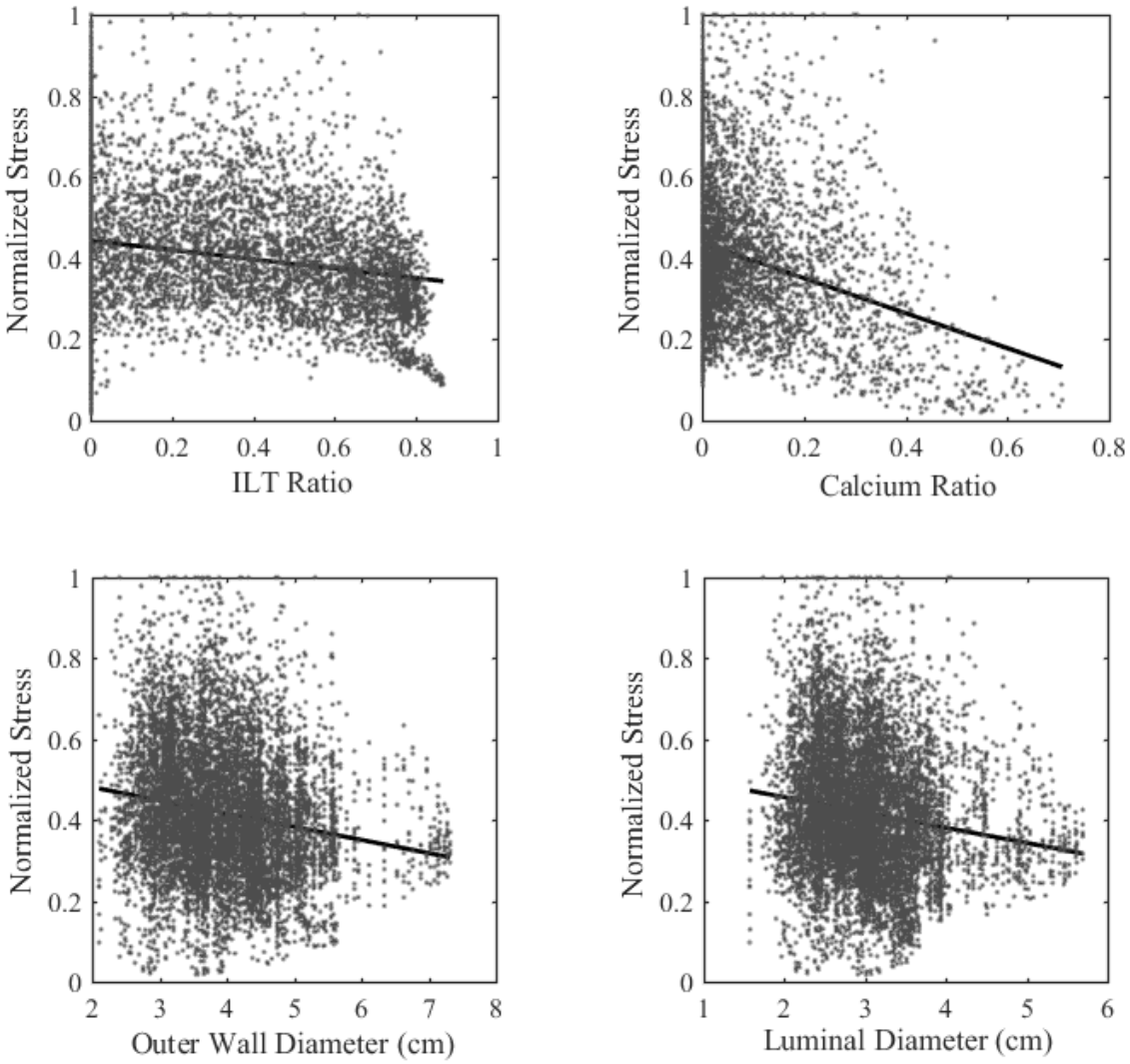

Figure S1. Association between stress and aneurysmal compositional and geometric features (A: Normalized stress vs ILT ratio; B: Normalized stress vs calcium ratio; C: Normalized stress vs outer wall diameter; and D: Normalized stress vs luminal diameter)

If the calcium and ILT were treated as wall, the stress distribution changed dramatically. The high stress concentration beneath the thick ILT layer, observed in Figure S2A and D, disappeared due to this over-simplification. Similar observations were seen in this study, where the stress level in ILT was low due to it being a softer material[6] and calcium undertook high stress loading due to its stiffer nature[4]. In order to accurately calculate the stress distribution within AAA wall, both ILT and calcium should be considered.

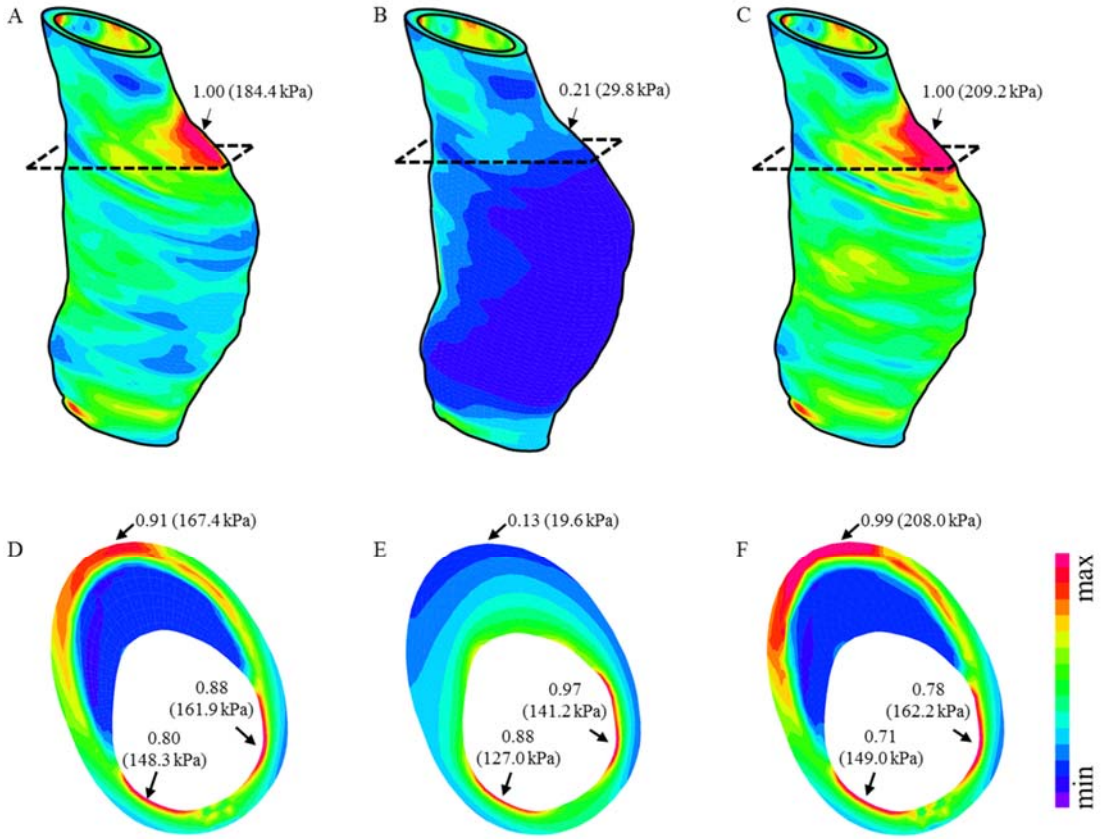

Figure S2. Stress distributions with different modeling assumptions. Upper panel: band plot on 3D geometry: (A) the model with uniform wall thickness and inclusion of components; (B) the model with uniform wall thickness but treating ILT and calcium as wall; and (C) the model with variable wall thickness and inclusion of components. Lower panel (D-F) shows the corresponding band plot on the transverse plane.

To better understand the influence of variations in wall thickness, a sensitivity analysis with models of both uniform and variable wall thickness (UWT and VWT, respectively) was performed. Compared with the VWT simulation, the stresses calculated in the UWT model showed excellent correlation (Figure S2C and F) with only a slight underestimation (slope=1.008, intercept=-5.5kPa, Pearson r=0.94, $p<0.0001$, Figure S3).

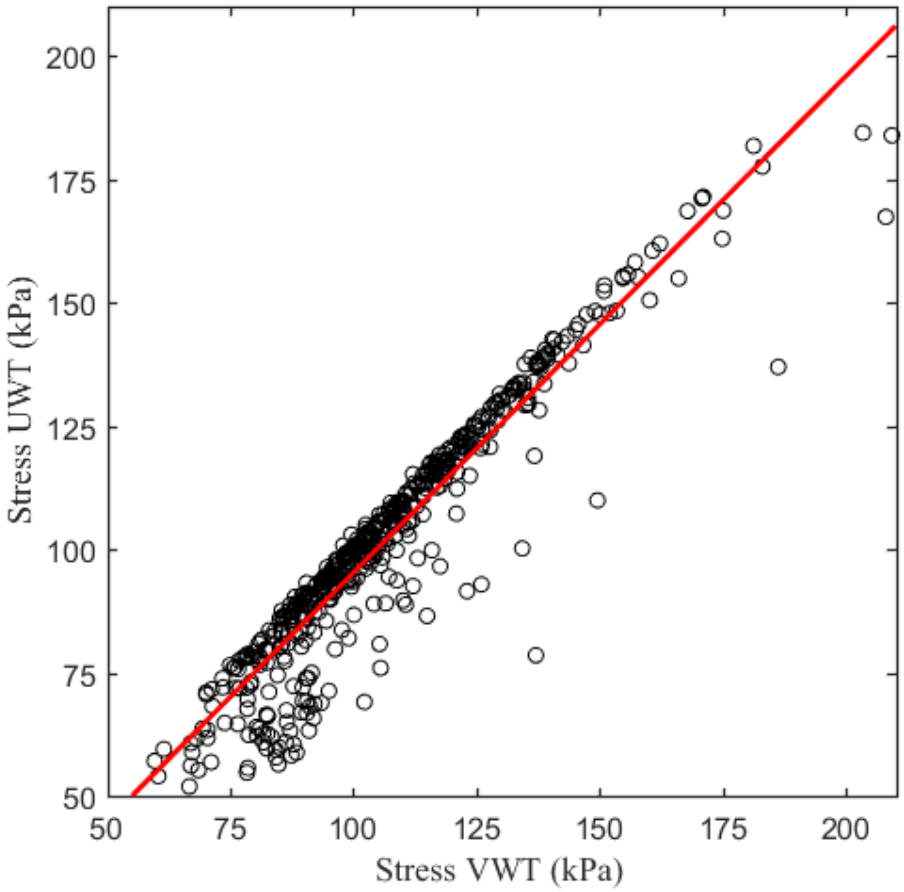

Figure S3. Correlation between stress values based on the assumption of uniform (UWT) and variable wall thickness (VWT).

Supplemental References

1. Maki-Petaja KM, Elkhawad M, Cheriyan J, Joshi FR, Ostor AJ, Hall FC, Rudd JH and Wilkinson IB. Anti-tumor necrosis factor-alpha therapy reduces aortic inflammation and stiffness in patients with rheumatoid arthritis. *Circulation*. 2012;126:2473-80.
2. Rudd JH, Warburton EA, Fryer TD, Jones HA, Clark JC, Antoun N, Johnstrom P, Davenport AP, Kirkpatrick PJ, Arch BN, Pickard JD and Weissberg PL. Imaging atherosclerotic plaque inflammation with [18F]-fluorodeoxyglucose positron emission tomography. *Circulation*. 2002;105:2708-11.
3. Teng Z, Feng J, Zhang Y, Huang Y, Sutcliffe MP, Brown AJ, Jing Z, Gillard JH and Lu Q. Layer- and Direction-Specific Material Properties, Extreme Extensibility and Ultimate Material Strength of Human Abdominal Aorta and Aneurysm: A Uniaxial Extension Study. *Ann Biomed Eng*. 2015;43:2745-59.
4. Maier A, Gee MW, Reeps C, Eckstein HH and Wall WA. Impact of calcifications on patient-specific wall stress analysis of abdominal aortic aneurysms. *Biomechanics and modeling in mechanobiology*. 2010;9:511-21.
5. Ebenstein DM, Coughlin D, Chapman J, Li C and Pruitt LA. Nanomechanical properties of calcification, fibrous tissue, and hematoma from atherosclerotic plaques. *Journal of biomedical materials research Part A*. 2009;91:1028-37.
6. Wang DH, Makaroun MS, Webster MW and Vorp DA. Effect of intraluminal thrombus on wall stress in patient-specific models of abdominal aortic aneurysm. *Journal of vascular surgery*. 2002;36:598-604.